Real-Time Monitoring for Road-Base Quality with the Aid of Buried Piezoelectric Sensors

Yuanqiang Cai[1], Li Ma[1], Zhigang Cao[1,*], Chunli Zhang[2], Guangya Ding[3], Quanyang Dong[3], Xueyu Geng[4], Taotao Yue[5]

1. Research Center of Coastal and Urban Geotechnical Engineering, Zhejiang University, Hangzhou, China

2. Key Laboratory of Soft Machines and Smart Devices of Zhejiang Province and Department of Engineering Mechanics, Zhejiang University, Hangzhou, China

3. College of Civil Engineering and Architecture, Wenzhou University, Wenzhou, China

4. School of Engineering (F332), The University of Warwick, Coventry, UK

5. China Railway 16 Bureau Group Beijing Metro Engineering Construction Co LTD, Beijing, China

***Corresponding author**

Zhigang Cao, Research Center of Coastal and Urban Geotechnical Engineering, Zhejiang University, E-mail address: caozhigang2011@zju.edu.cn

Abstract: The road-base usually deteriorate during service time due to factors such as cyclical traffic loads and road-base fouling. Currently the monitoring method for road-base quality is quite limited. This paper proposes a real-time Monitoring method for Road-Base Quality (MRBQ) based on a soil dynamic model and piezoelectric sensors buried in road-base. The soil dynamic model was extended with a piezoelectric equation to calculate the voltage in the road-base generated by a moving traffic load. Then, a model test was conducted to measure the output voltage of the piezoelectric sensors buried in the road-base. Finally, the road-base modulus was back-calculated through the soil dynamic model with the measured voltage. The back-calculated modulus was compared with the modulus measured by resonance column test (RCT) to validate this method. The unique relationship between the peak voltage and the road-base modulus at various depths was identified for different traffic load amplitudes and speeds, and the feasibility and accuracy of the MRBQ was demonstrated. This study reveals that the sensitivity of the piezoelectric sensors can reach 2 V/MPa, and the error to measure the road-base modulus is less than 20%. The proposed MRBQ demonstrates a good application potential in health monitoring of transportation facilities.

Keywords: Road-base quality, Elastic modulus, Real-time monitoring, Traffic load, Piezoelectric sensor

Introduction

In recent years, the maintenance of transportation facilities have become increasingly important due to the rapid increase of mileage of transportation facilities being put into operation. The deterioration of the road-base can be caused by factors such as cyclical traffic load and road-base fouling (Cao et al.,2018; Danesh et al.,2018). Currently, the monitoring method which can realize the real-time monitoring of the quality of transportation facility is relatively limited.

The elastic modulus is a major indicator of road-base quality, which can be used as one index in the road-base quality monitoring. Traditional detection methods to obtain the road-base modulus include the falling weight deflectometer (FWD) and the Rayleigh velocity back-calculation method. As early as in 1968, Scrivner et al.(1968) from the Texas Transportation Institute first proposed the method of back-calculation the modulus using a FWD bent sunken basin based on Burmister's two-layer solution system. In 1979, Lytton (1989) suggested the back-calculation of the modulus of a rigid underlying layer and devised a back-calculation program. In the last 20 years, researches (Malla and Joshi,2008; Sun et al.,2016) have improved the modulus back-calculation methodology using a more accurate model. On the other hand, Ummin et al.(2013) adopted the Rayleigh wave for the nondestructive testing of roads and Jia and Li (2012) performed a back-calculation of the road-base modulus by the measured Rayleigh wave velocity. However, all of the above methods use a drop hammer as the excitation input, and thus the road-base modulus cannot be acquired in real time.

In recent years, some scholars have proposed the concept of an active sensor (Jin et al.,2019; Wang,2013) which is defined as a sensor generating electrical signals as a response to external changes without an external power source (Wang et al.,2015). Based on this definition, Zhao et al.(2017) created a vibration sensor based on nanomaterials. Both theoretical and experimental analyses confirmed that the output voltage and acceleration were linearly sensitive, which enabled the sensor to monitor railway acceleration. Yu et al.(2017) also used sensors made of nanomaterials to monitor bridge health, including displacement and acceleration. Wang et al.(2017) created a sensor to collect wind energy, and the relationship between the voltage output and wind speed was found to be linearly. Sensors made of piezoelectric materials are also widely used. Zhang et al.(2015) have studied the influence of Winkler road-base modulus on the output of piezoelectric transducer under traffic load. Lin et al.(2013) used piezoelectric materials to create an energy collector to monitor both the traffic's speed and weight based on its mechanical-electrical coupling. The above studies confirm that smart materials can be fabricated into active sensors to monitor the healthy state of a transportation facility in real-time based on the relationship between the output voltage and external traffic loads.

In terms of transportation monitoring, Xue et al.(2014) proposed a pavement health monitoring system based on an embedded sensing network and the modulus of the pavement surface layer can be back-calculated based on testing runs and numerical models. Kafle et al.(2017) have done a good work in bridge health monitoring. In their study, an integrated bridge health monitoring framework using advanced 3D Finite

Element modeling was developed and the realistic traffic loads imposed on the bridge can be obtained based on Weight-in-motion (WIM) technology and interferometric radar sensors (IBIS-S). However, previous researches focus more on the structures above the road pavement and currently there is no feasible real-time monitoring method suitable for the road-base quality as it is a hidden structure beneath the pavement. Vibrations of the road-base and ground can be induced by the moving traffic load, which may be used as a signal for real-time monitoring. Using the soil dynamic model, Auersch (1996), Bo (2004), and Cai et al.(2007) predicted the dynamic response of both the road-base and the ground when subjected to a moving traffic load. It was found that the dynamic stress, displacement, and velocity of the road-base generated by the moving traffic loads relate to the parameter of road-base as well as the traffic loads. This inspired the authors to establish a real-time monitoring method for road-base quality (MRBQ) based on the relationship between the road-base modulus and its dynamic response. In the intelligent transportation system (ITS), the modulus of a road-base is one major indicator of its quality. The road-base modulus deteriorates during its service time when subjected to loads from the external environment. Thus, there is a strong need to develop a real-time monitoring method of road-base to facilitate the timely and economic maintenance of ITS.

To meet these challenges, this paper first proposes a real-time monitoring method for road-base quality (MRBQ) based on the soil dynamic model previously developed by the authors (Cai et al.,2009) and the piezoelectric sensors buried in the road-base. The implementation process of the MRBQ is presented in Fig. 1. First, the piezoelectric

sensors are arranged in the road-base for the intelligent road system. Then, the voltage signal induced by the moving traffic loads is collected by the piezoelectric sensors. Finally, the road-base elastic modulus can be back-calculated through the theoretical model with the measured voltage signal. Therefore, the real-time monitoring of road-base elastic modulus could be achieved in different traffic environments and road-base conditions.

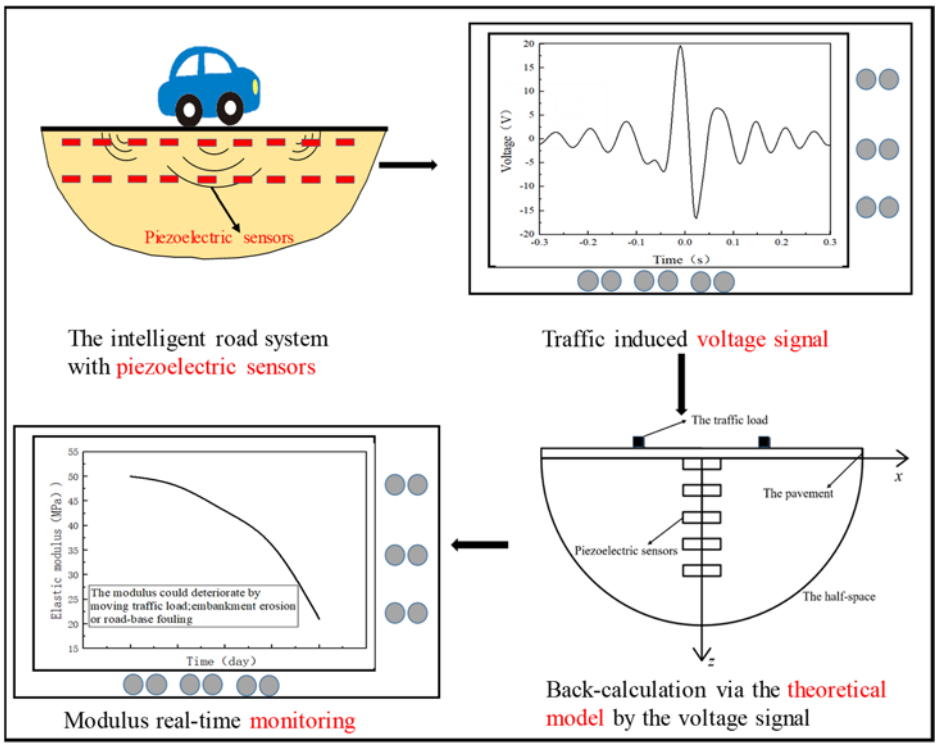

Fig. 1 The implementation process of the MRBQ

The paper is organized in the following order. Firstly, the soil dynamic model is extended with a piezoelectric equation to calculate the voltage in the road-base generated by a moving traffic load. Then, the unique relationship between the peak voltage and the road-base modulus at various depths within the road-base was identified for different traffic loads and traffic speeds. Then, a model test for the road-base under an excitation load is performed to measure the output voltage of the piezoelectric sensors under different road-base modulus and a resonance column test (RCT) is

conducted to measure the road-base modulus. Finally, a comparison between the back-calculated and measured road-base modulus verifies the feasibility and accuracy of the proposed MRBQ.

The Soil Dynamic Model

Based on the soil dynamic model previously developed by the authors (Cai et al.,2009), this paper established a theoretical model which was extended via the piezoelectric sensors, as shown in Fig. 2. Four rectangular moving traffic loads simulate the vehicle. A Kirchhoff plate is used to simulate the asphalt pavement layer, and the poroelastic half-space governed by Biot's theory (1956) is utilized to simulate the road-base. Piezoelectric sensors (made by piezoelectric ceramic) are placed every 20 cm in the road-base depth, assuming that the sensors are in full contact with the soil (the sensor is much harder than soil).

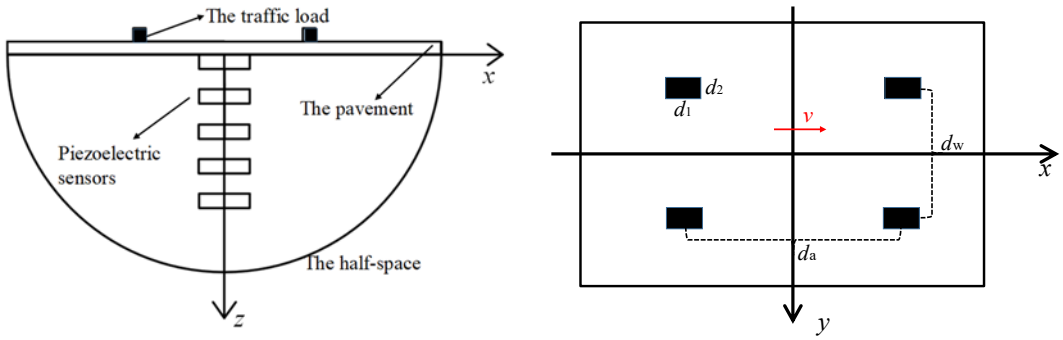

Fig. 2 The theoretical model

The Governing Equations and Solutions

The soil dynamic equation of the half-space is presented as follows (Biot,1956):

$$\mu u_{i,jj} + (\lambda + \alpha^2 M + \mu) u_{j,ji} + \alpha M w_{j,ji} = \rho \ddot{u}_i + \rho_f \ddot{w}_i \tag{1}$$

$$\alpha M u_{j,ji} + M w_{j,ji} = \rho_{\mathrm{f}} \ddot{u}_i + m\ddot{w}_i + b\dot{w}_i \tag{2}$$

In the above equation, u_i $(i = x, y, z)$ is the displacement of the soil skeleton along the x, y, and z directions, respectively. w_i $(i = x, y, z)$ is the displacement of liquid relative to the soil skeleton along the x, y, and z directions; α and M are soil parameters representing the compressibility of soil particles and pore fluids. ρ and ρ_{f} are the densities of the soil and liquid phases, respectively. $m = \rho_{\mathrm{f}}/\mathrm{n}$ represents the parameter of soil porosity, n is the porosity of soil mass, and b is the physical quantity of the internal friction when the fluid–solid relative displacement is reflected. The points above u_i and w_i represent the derivative with respect to time t. λ and μ are the Láme constants. μ is the shear modulus.

The stress-strain relationship of the soil is written as:

$$\sigma_{ij} = \lambda \delta_{ij} \theta + \mu(u_{i,j} + u_{j,i}) - \alpha \delta_{ij} P_{\mathrm{f}} \tag{3}$$

$$P_{\mathrm{f}} = -\alpha M \theta + M\varsigma \tag{4}$$

where $\theta = u_{i,i}$ is the volumetric strain of the soil and σ_{ij} is the total stress of the soil mass. P_{f} is the pore water pressure, and δ_{ij} is the Dirac delta function. The governing equation of the Kirchhoff plate is introduced as:

$$D_{\mathrm{p}}\left[\frac{\partial^4 w(x,y,t)}{\partial x^4} + 2\frac{\partial^4 w(x,y,t)}{\partial x^2 \partial y^2} + \frac{\partial^4 w(x,y,t)}{\partial y^4}\right] + m_{\mathrm{p}} \frac{\partial^2 w(x,y,t)}{\partial t^2} = q(x,y,t) + F(x,y,t) \tag{5}$$

where w is the vertical displacement of the plate, m_{b} is the mass per unit area of the plate, $q(x, y, t)$ is the moving load, $F(x, y, t)$ is the force exerted on the plate by the underlying soil mass, D_{p} is the stiffness of the elastic plate, and E, h_{p}, and ν_{p} are the elastic

modulus, thickness, and the Poisson ratio of the plate, respectively.

The four rectangular moving traffic loads are introduced as follows:

$$q(x,y,t)=\begin{cases} q_0 & \frac{d_a-d_1}{2}\le |x-vt|\le \frac{d_a+d_1}{2} \text{ and } \frac{d_w-d_2}{2}\le |y|\le \frac{d_w+d_2}{2} \\ 0 & \text{others} \end{cases} \tag{6}$$

where q_0 is the traffic load amplitude; the meaning of d_a, d_w, d_1, d_2 could be referred to Fig. 2.

The detailed derivation process of the poroelastic half-space and the meaning of the specific parameters in the above equation can be referenced in the work by Cai et al.(2015). The final solution is obtained as follows:

$$\tilde{\tilde{\tilde{\sigma}}}_z=\frac{\tilde{\tilde{\tilde{q}}}(\xi,\eta,\omega)\phi'(\xi,\eta,z,\omega,\mu)}{\phi(\xi,\eta,0,\omega,\mu)[D_p(\xi^2+\eta^2)^2-m_p\omega^2]+1} \tag{7}$$

The Governing Equations for the Buried Piezoelectric Sensor

Then the piezoelectric equation is introduced as:

$$D=d_{33}\sigma_z(x,y,z,t)+\varepsilon_{33}E_z(x,y,z,t) \tag{8}$$

where D is the electrical displacement, d_{33} is the piezoelectric constant of piezoelectric ceramic,σ_z is the vertical soil stress, ε_{33} is the relative dielectric constant, and Ez is the electric field intensity.

$$\varepsilon_{33}=\varepsilon_r\varepsilon_0 \tag{9}$$

where ε_r is the relative permittivity and ε_0 is the vacuum permittivity.

The electric field intensity is defined as:

$$E_{\mathrm{z}}(x,y,z,t) = -\frac{V(x,y,z,t)}{h} \tag{10}$$

where h is the thickness of the piezoelectric ceramic and V is the output voltage of the piezoelectric ceramic.

By applying the surface integral of equation (8), the following equation is obtained:

$$Q = \iint D dS = d_{33}\sigma_{\mathrm{z}}(x,y,z,t)S + \varepsilon_{33}E_{\mathrm{z}}(x,y,z,t)S \tag{11}$$

where Q is the charge of the piezoelectric ceramic and S is the area of the piezoelectric ceramic. If the piezoelectric ceramic is connected to the external resistance R_{L}, according to Gauss's theorem, the output of the electric current is the following：

$$I = \frac{dQ}{dt} = \frac{V(x,y,z,t)}{R_{\mathrm{L}}} \tag{12}$$

Consequently, the following equation is obtained:

$$d_{33}S\frac{\partial\sigma_{\mathrm{z}}(x,y,z,t)}{\partial t} = \frac{\varepsilon_{33}S}{h}\frac{\partial V(x,y,z,t)}{\partial t} + \frac{V(x,y,z,t)}{R_{\mathrm{L}}} \tag{13}$$

To solve the differential equation of equation (13), its triple Fourier transform can be obtained as follows:

$$d_{33}S(i\omega)\overline{\overline{\widetilde{\sigma}_{\mathrm{z}}}}(\xi,\eta,z,\omega) = i\omega C_{\mathrm{p}}\overline{\overline{\widetilde{V}}}(\xi,\eta,z,\omega) + \frac{1}{R_{\mathrm{L}}}\overline{\overline{\widetilde{V}}}(\xi,\eta,z,\omega) \tag{14}$$

where

$$C_{\mathrm{p}} = \frac{\varepsilon_{\mathrm{r}}\varepsilon_0 S}{h} \tag{15}$$

Therefore, the following equation can be obtained:

$$\overline{\overline{\widetilde{V}}}(\xi,\eta,z,\omega) = \Psi(\omega)\overline{\overline{\widetilde{\sigma}_{\mathrm{z}}}}(\xi,\eta,z,\omega) \tag{16}$$

where

$$\Psi(\omega) = \frac{d_{33} S(i\omega)}{\frac{1}{R_{\mathrm{L}}} + i\omega C_{\mathrm{p}}} \tag{17}$$

Then, put N piezoelectric ceramic in series and substitute equation (7) into equation (16):

$$\bar{\bar{\bar{V}}}(\xi, \eta, z, \omega) = N\Psi(\omega) \frac{\bar{\bar{\bar{q}}}(\xi,\eta,\omega)\phi'(\xi,\eta,z,\omega,\mu)}{\phi(\xi,\eta,0,\omega,\mu)[D_{\mathrm{p}}(\xi^2+\eta^2)^2 - m_{\mathrm{p}}\omega^2]+1} \tag{18}$$

Finally, the time-domain voltage of the piezoelectric sensor is obtained by the inverse Fourier transformation:

$$V(x, y, z, t) = \frac{1}{4\pi^2} \iint N\Psi(-\xi v) \frac{\bar{\bar{q}}(\xi,\eta)\phi'(\xi,\eta,z,-\xi v,\mu) e^{i(\xi x+\eta y-\xi v t)} d\xi d\eta}{\phi(\xi,\eta,0,-\xi v,\mu)[D_{\mathrm{p}}(\xi^2+\eta^2)^2 - m_{\mathrm{p}}(-\xi v)^2]+1} \tag{19}$$

The Dynamic Stress and Voltage Response

The parameters of λ and μ are the Láme constants, and μ is the shear modulus. The complex elastic modulus was introduced to consider the damping of soil: $\mu = \mu^0(1 + 2iD_1)$，$\lambda = 2\mu\nu/（1 - 2\nu）$. D_1 is the damping ratio with a value of 0.05. The elastic modulus of the plate can be expressed as：$E = E^0(1 + 2iD_2)$, where D_2 is the plate's damping ratio (D_2 = 0.002). The parameters of the poroelastic half-space are shown in Table 1. The parameters for the moving traffic loads, the Kirchhoff plate, and the piezoelectric sensor are presented in Tables 2, 3, and 4, respectively to illustrate the model.

Table 1 The parameters of the road-base

Parameters	Value
The shear modulus of the road-base, μ^0 (MPa)	25
The density of the soil skeleton, ρ_s (kg/m^3)	1816
The density of the liquid phases, ρ_f (kg/m^3)	1000
The porosity of soil mass, n	0.4

The physical quantity of the internal friction, b (N.s/m^4)	1.73×10^5
The compressibility of soil particles, α	1
The poisson's ratio of the soil, ν	0.35
The compressibility of pore fluids, M (MPa)	240

Table 2 The parameters of moving traffic load

Parameters	Value
The traffic load amplitude, q_0 (kPa)	500
d_1 (m)	0.2
d_2 (m)	0.2
d_w (m)	1.5
da (m)	3
The traffic speed, v (m/s)	25

Table 3 The parameters of Kirchhoff plate

Parameters	Value
The elastic modulus of the asphalt pavement, E^0 (10^9 Pa)	3.5
The poisson's ratio of the asphalt pavement, ν_p	0.15
The mass per unit area, m_p (kg/m^2)	350
The thickness of the asphalt pavement, h_p (m)	0.35

Table 4 The parameters of piezoelectric sensor

Parameters	Value
Piezoelectric constant, d_{33} (C/N)	600×10^{-12}
The area of the piezoelectric ceramic, S (m^2)	$2\times2\times10^{-4}$
The number of stacked ceramics, N (a)	10
The thickness of the piezoelectric ceramic, h (m)	1×10^{-3}
The relative permittivity,ε_r (F/m)	3000
The vacuum permittivity,ε_0 (F/m)	8.854×10^{-12}
The external resistance, R_L (MΩ)	10

The output soil stress and voltage of the piezoelectric sensors generated by moving traffic loads under different road-base modulus are first presented. Fig. 3(a) shows the soil-stress time history curve with three different soil elastic modulus under a moving traffic load. It is evident that a vehicle movement induces one positive stress peak and two negative stress peaks. However, an increase in the road-base elastic modulus causes a decrease in the stress peak, and the stress time history curve becomes smoother. This can be explained by the fact that increasing the road-base modulus also increases overall

stiffness of the road-base; this is equivalent to reducing the road-base reaction, thereby reducing soil stress.

Fig. 3(b) shows the output voltage time history curve with three different elastic modulus under a moving traffic load. It is evident that the output voltage time history curve has one positive voltage peak and one negative voltage peak. When comparing Fig. 3(a) with Fig. 3(b), a time deviation between the peak voltage and the peak stress is revealed, and it is because the voltage is not only related to the stress amplitude, but also to the rate of stress change (in equation [13]:$\frac{\partial \sigma_z}{\partial t}$). It is worth noting that the peak voltage occurs near the center of the vehicle. The peak voltage is 19.7 V when the elastic modulus is 20 MPa; it decreases to 16.2 V for an elastic modulus at 25 MPa and decreases again to 12.3 V for an elastic modulus at 30 MPa. It can thus be concluded that the peak voltage increases with a reduction of the elastic modulus. This phenomenon provides a theoretical basis for the monitoring of road-base modulus by the peak voltage of piezoelectric sensors.

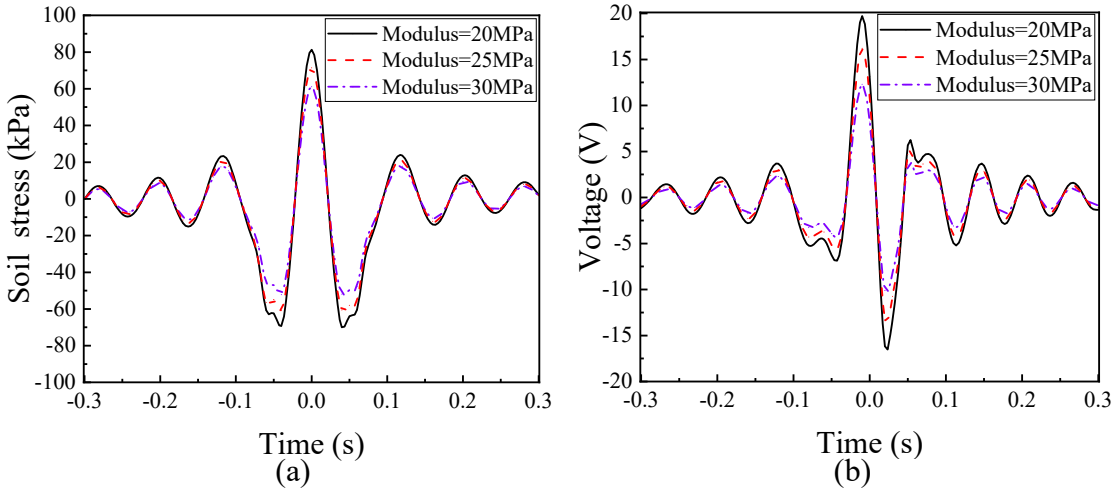

Fig. 3 The influence of elastic modulus on (a) Soil Stress and (b) Voltage

Fig. 4 reveals that the peak voltage has a unique mapping relationship with the soil's elastic modulus. This relationship can be obtained from the soil dynamic theory and the piezoelectric theory presented in (The Soil Dynamic Model). Furthermore, the peak voltage increases as the elastic modulus decreases; when the traffic speed is 25 m/s, traffic load is 112 kN, and buried depth is 0 m, the sensitivity (the slope of the relation curve) can reach about 2 V/MPa, which is very high in the context of sensors. Fig. 4 also presents the influence of traffic speed and traffic-load amplitude at various buried depths on the output voltage. This indicates that the piezoelectric sensors have a wide range of adaptability in monitoring the elastic modulus of road-bases under different circumstances.

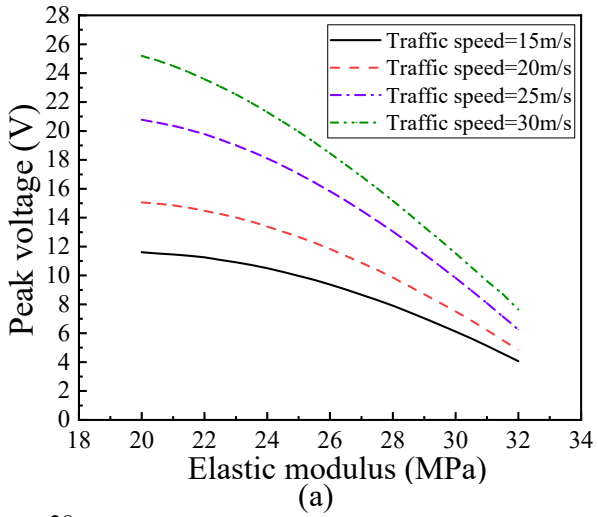

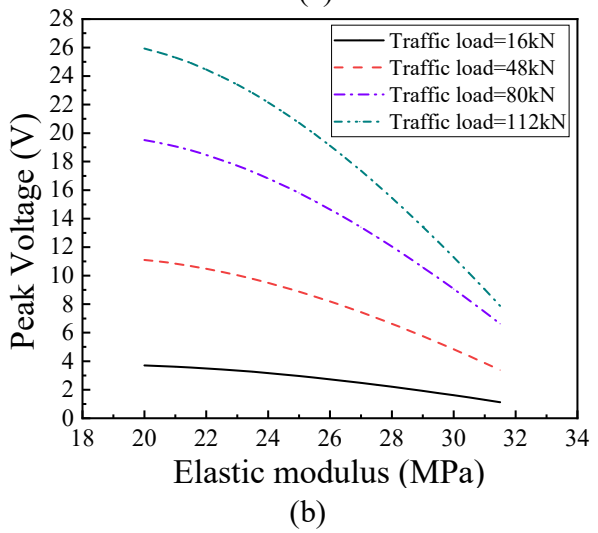

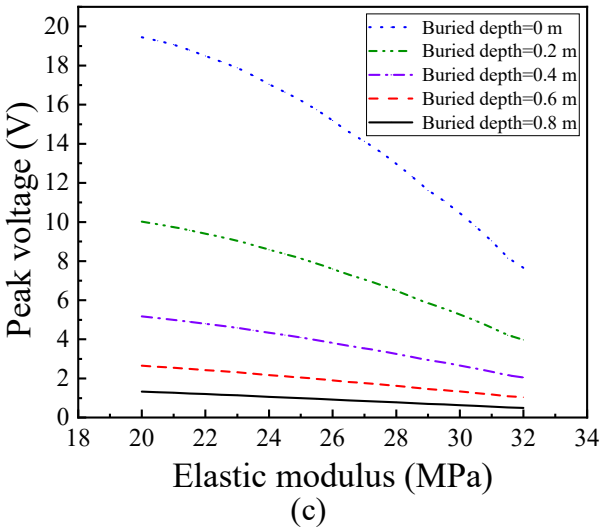

Fig. 4 The influence of (a) traffic speed; (b) traffic load; and (c) buried depth on the relationship curve

Laboratory Tests

In (**The Soil Dynamic Model**) and (**The Dynamic Stress and Voltage Response**), the output voltage in the road-base under a moving traffic load was calculated through the theoretical model and the unique relationship between the peak voltage and the road-base elastic modulus was identified. In this section, a model test (as shown in Fig. 7) conducted to measure the output voltage by the piezoelectric sensors under a dynamic traffic load as well as the Resonance Column Test (RCT) (as shown in Fig. 8) to measure the road-base elastic modulus is introduced.

The Road-Base Model Test

The calibration test of the piezoelectric sensor

The piezoelectric sensors are made of self-purchased stacked piezoelectric ceramics. The parameters of the piezoelectric sensor (stacked piezoelectric ceramic), which include the piezoelectric constant d_{33}, the size of the piezoelectric sensor, the external resistance R_L, the number of stacked ceramics, are listed in Table 5.

Table 5 The parameters of piezoelectric sensor (stacked piezoelectric ceramic)

Parameters	Value
Piezoelectric constant, d_{33} (C/N)	600×10^{-12}
The area of the piezoelectric ceramic, S (m^2)	$2\times2\times10^{-4}$
The number of stacked ceramic, N (a)	10
The thickness of the piezoelectric ceramic, h (m)	1×10^{-3}
The relative permittivity,ε_r (F/m)	3000
The vacuum permittivity,ε_0 (F/m)	8.854×10^{-12}
The external resistance, R_L (MΩ)	10
The density of piezoelectric ceramics, ρ_P (kg/m^2)	7.5×10^3
The stiffness of piezoelectric ceramics, E (N/m^2)	56×10^9

In Fig. 5, the vibrator is used to apply excitation load for the piezoelectric sensor and the voltmeter is used to measure the output voltage. The excitation load amplitudes are 8 N, 12 N, 16 N, 20 N and 24 N (the internal stresses of the sensor are 20 kPa, 30 kPa, 40 kPa, 50 kPa and 60 kPa), the excitation frequency is 9 Hz.

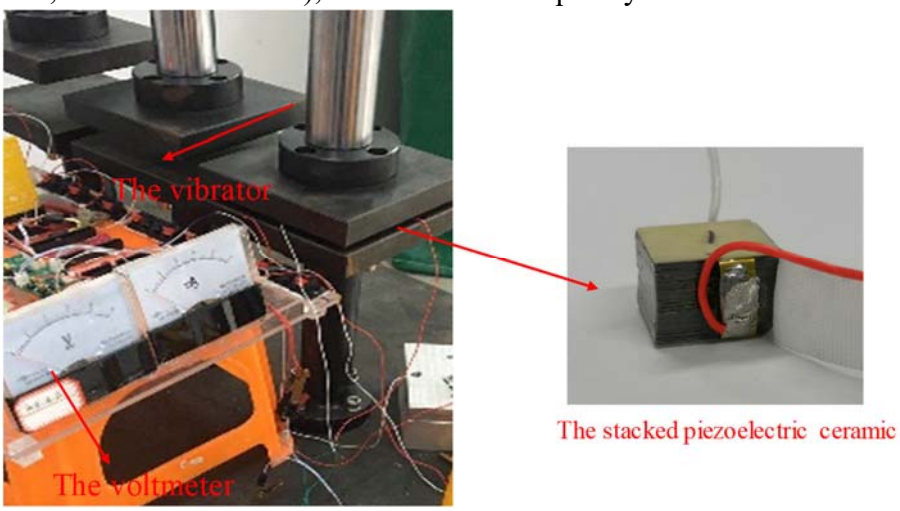

Fig. 5 The calibration test

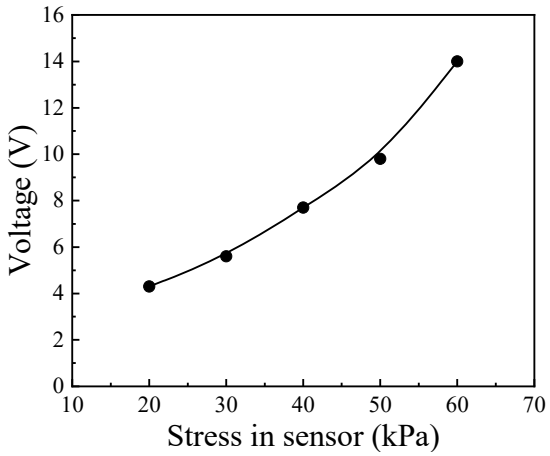

Fig. 6 The calibration curve of the piezoelectric sensor

Fig. 6 shows that the calibration curve between the stress and the output voltage is almost linear.

The model test setup

The model test, as shown in Fig. 7(a), comprised an excitation hammer, a rubber sheet (under the hammer), an asphalt pavement, five piezoelectric sensors, five soil-pressure boxes, and the lime-soil road-base. The rubber sheet has the size of 0.1 m× 0.1 m. The depths of the asphalt pavement was 20 cm. The depth of the lime-soil road-base was 1 m. The piezoelectric sensors were made of stacked piezoelectric ceramic (as shown in Fig. 7b and Fig. 7c) and were placed in the road-base at the epicenter. The distance between them is 0.2 m as well as the five soil-pressure boxes.

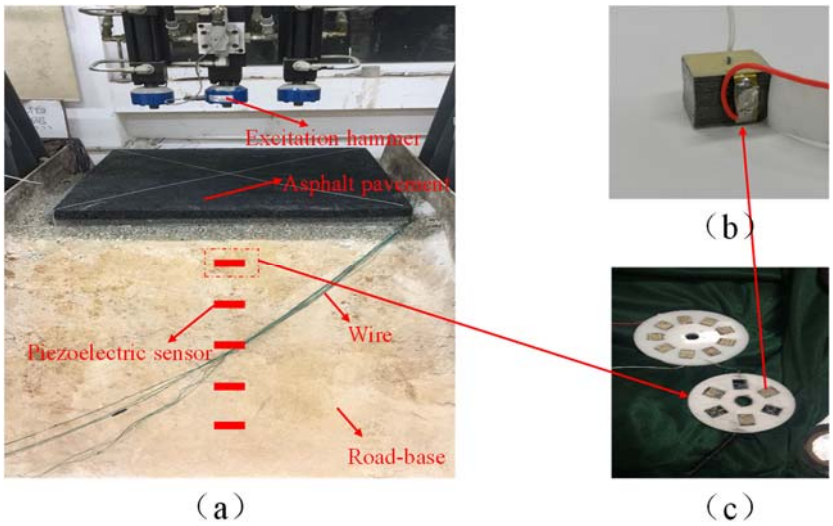

Fig. 7 The model test: (a) The model test setup; (b) The stacked piezoelectric ceramic; (c) The stacked piezoelectric ceramic after packaging (piezoelectric sensor)

The relevant parameters of the asphalt pavement and road-base are listed in Table 6 and Table 7, respectively.

Table 6 The parameters of asphalt pavement

Parameters	Value
The elastic Modulus of the asphalt pavement, E^0 (10^9 Pa)	3.5
The poisson's ratio of the asphalt pavement, ν_p	0.15
The mass per unit area, m_p (kg/m^2)	350
The thickness of the asphalt layer, h_p (m)	0.30

Table 7 The parameters of lime-soil road-base

Parameters	Value
The degree of compaction (%)	90
The water content (%)	4.2
The density (kg/m^3)	1500
The thickness of the lime-soil road-base, h_s (m)	1

In this test, the excitation hammer (excitation load amplitude range: 1 kN to 5 kN, and frequency range: 1 Hz to 15 Hz) was used to simulate the cyclic traffic load. The rubber sheet was used to simulate vehicle tires. The soil-pressure boxes was used to measure the dynamic stress, whereas the piezoelectric sensors to measure the electric response (output voltage) in the road-base under the dynamic traffic load.

The road-base testing materials

The lime soil was used as the road-base in the model test. It is noteworthy that the elastic modulus of lime soil changes over time (the water in the lime soil gradually reacts with lime).

The shear modulus of the road-base in the model test was measured by the resonance column, as shown in Fig. 8(c); the soil specimen (Fig. 8b) used in the RCT was sampled from the road-base as depicted in Fig. 8(a). In each measurement, we took three soil samples at z = 0.5 m for the RCT.

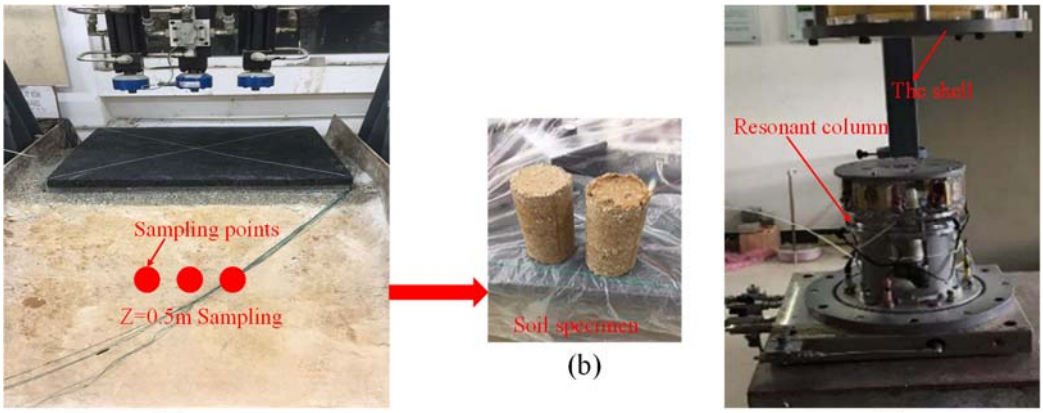

Fig. 8 Resonance Column Test (RCT): (a) Soil sampling; (b) Soil specimen; (c) Resonance column

Finally, the elastic modulus of the road-base on the 1st day, 7th day, and 14th day was measured by the resonance column test. Fig. 9 reveals that the elastic modulus of road-base changes over time. In each measurement, the elastic modulus of the three samples was approximately the average values of about 23 MPa, 29 MPa, and 34 MPa, respectively, on the 1st day, the 7th day, and the 14th day.

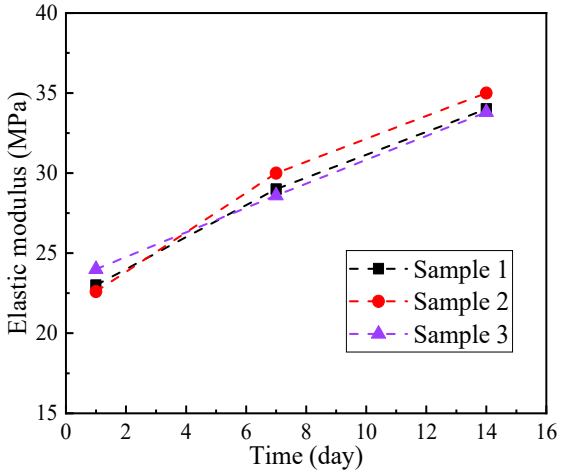

Fig. 9 The elastic modulus of road-base changes over time

Testing Results

The dynamic stress in the road-base and electric responses of the piezoelectric sensor were measured under the cases of different road-base modulus. The influence of

road-base modulus on soil stress and output voltage is analyzed under different conditions (such as different excitation-load amplitudes, varying excitation frequencies, and different sensor depths) in the following section.

The dynamic stress and output voltage in the road-base

Fig. 10 presents the measured time history curve of the soil stress (a) and the output voltage (b) at z = 0 m for three two elastic modulus under an excitation load of 5 kN with excitation frequency 9 Hz. (The range of one wheel traffic load: 1 kN to 10 kN; the range of road-base vibration frequency caused by traffic load: 0 Hz to 15 Hz).

The peak stresses were 52 kPa and 41 kPa and the peak voltages were 12.2 V and 7.4 V for the soil elastic modulus of 23 MPa and 34 MPa, respectively. The significant impact of the road-base modulus on both dynamic and electric responses is confirmed by the test results. The reason for this phenomenon is explained in (The Dynamic Stress and Voltage Response) as the change of road-base modulus is equivalent to change the overall stiffness of the road-base; this is equivalent to reducing the road-base reaction, thereby reducing soil stress.

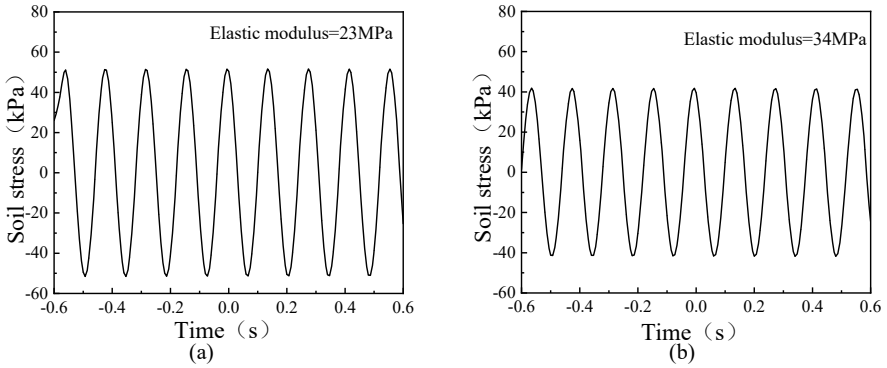

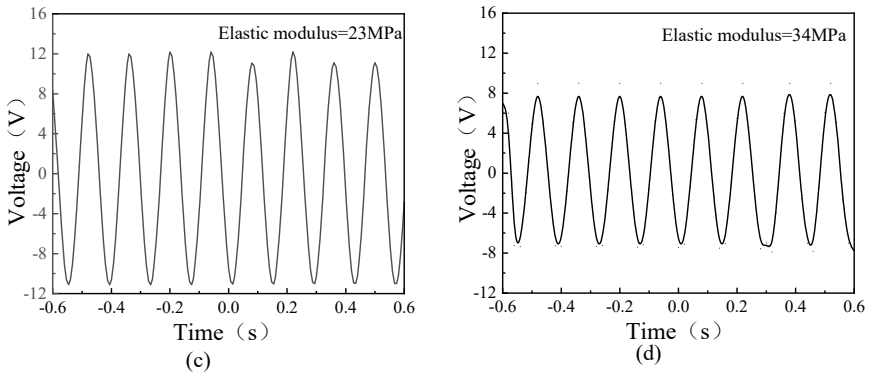

Fig. 10 The measured dynamic stress and output voltage in the road base

Fig. 11 presents the measured peak stresses and voltages at depths of z = 0 m, 0.2 m, 0.4 m, 0.6 m, and 0.8 m under an excitation load of 5 kN with the excitation frequency of 9 Hz. Both the peak stress and the peak voltage decrease greatly with depth, and nearly vanish at a depth of 0.8 m. Therefore, in the MRBQ, the piezoelectric sensors are suitable to bury in the road-base within 0.8 m. It is also clearly shown that an increase in road-base modulus reduces the peak voltage at various depth.

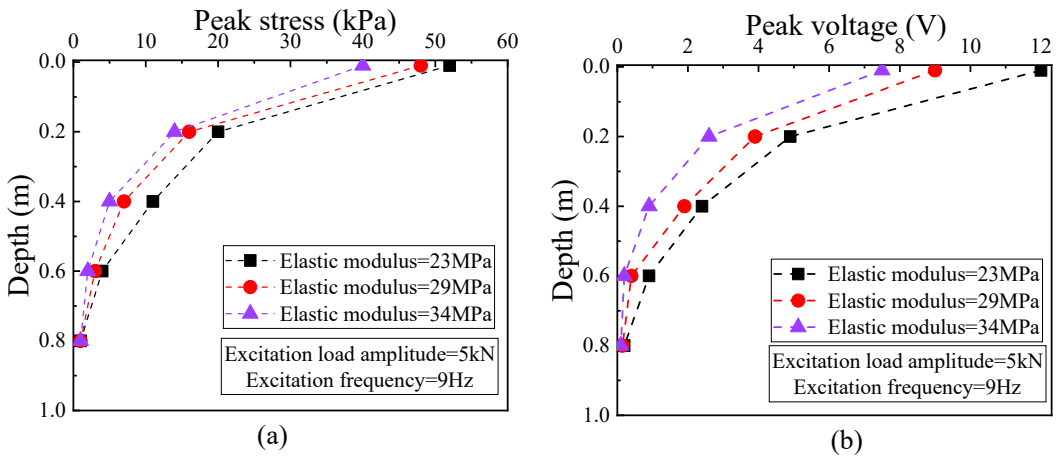

Fig. 11 The curve of (a) peak stress and (b) peak voltage with depth for three different soil modulus

Fig. 12 presents the measured peak voltage of the piezoelectric sensor at z=0 m under the excitation loads range of 1 kN to 5 kN and frequency range of 1 Hz to 15 Hz. The peak voltage is theoretically in linear relationship to the excitation load amplitude

according to the linearized piezoelectricity equations. While a close inspection to Fig.12 shows that the peak voltage is actually in nonlinear relationship with the load amplitude. This is due to the fact that the "soil arching" effects would occur in the experiments due to the different modulus of soil and sensors, which would result in errors in the measured results. These errors need to be calibrated through the unique relationship between the peak voltage excitation load amplitude to make sure the correctness of MRBQ, as shown in Fig. 12(a). According to Fig. 12(b), the peak voltage increases rapidly with the load excitation frequency. The sensitivity of peak voltage to excitation frequency will make MRBQ well used in traffic monitoring (low-frequency traffic condition). By the way, it is also clearly shown that the peak voltage increases when the elastic modulus decreases under various excitation-load amplitudes and frequencies.

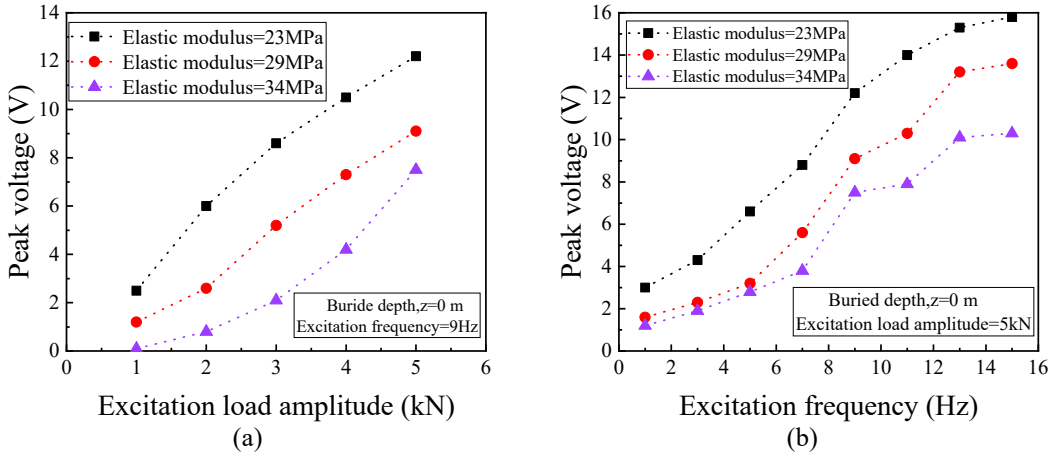

Fig. 12 The peak voltage against (a) excitation load amplitude and (b) frequency for three different soil modulus

Feasibility and Accuracy of the MRBQ

In the MRBQ, the piezoelectric sensors buried in the road-base can measure the electrical signals in quick response and high precision, and the soil dynamic model makes it possible to back-calculate the dynamic modulus with the electrical signal. So

this section performs a validation of the feasibility and accuracy of the MRBQ with the model test results. The validation process is outlined in Fig. 13. The output voltage of the piezoelectric sensor through the model test was obtained, and the road-base modulus was back-calculated through the soil dynamic model based on the output voltage. The elastic modulus of road-base was measured through the RCT. Finally, the back-calculated modulus through MRBQ were compared with the measured modulus by RCT, as shown in Table 8 and Fig. 14.

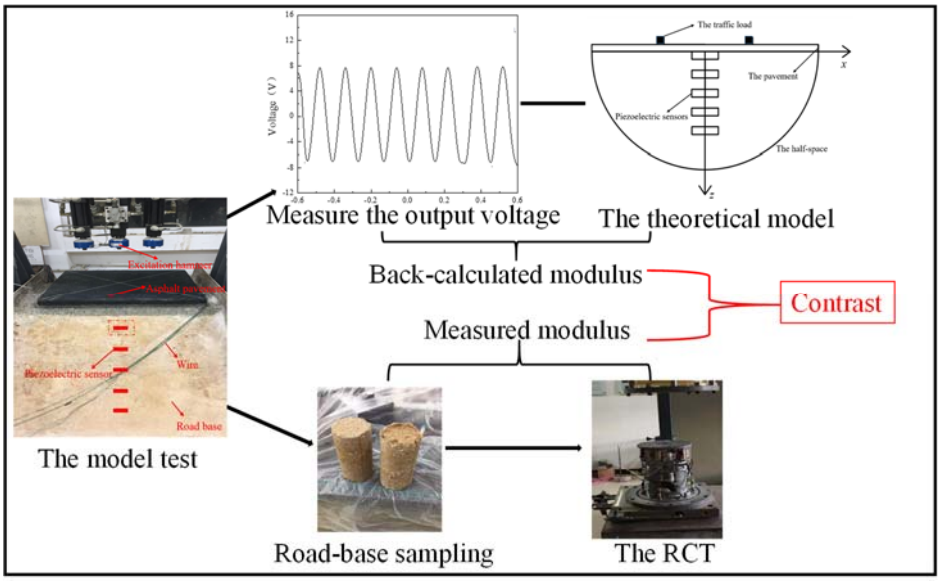

Fig. 13 The validation of the MRBQ

It is shown in Fig. 14(a) that with an increase in excitation-load amplitude, the back-calculated modulus become increasingly closer to the measured values. This is consistent with the theory in (**The Dynamic Stress and Voltage Response**) that the sensitivity of the piezoelectric sensor will increase with the amplitude of traffic load. Similarly, the elastic modulus in Fig. 14(b) were back-calculated with the peak voltage in Fig. 12(b). It is also evident that as the excitation frequency increases, the accuracy of the back-calculated modulus also increases. The error of the back-calculated

modulus is less than 20% and the accuracy can be improved as the excitation load amplitude and frequency increases. This indicates that the MRBQ has good application potential in the field of real-time road-base monitoring.

Table 8 The error between actual modulus and back-calculated modulus based on the MRBQ

The actual modulus(MPa)	The back-calculated modulus(MPa)	Error
23	24.2	5.2%
29	30	3.4%
34	34.6	1.8%

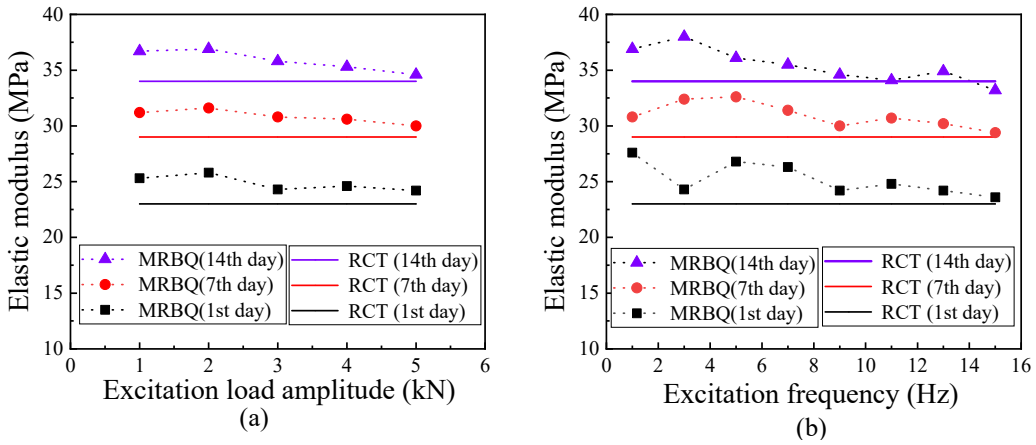

Fig. 14 The contrast of the elastic modulus (a) Different load amplitude; (b) Different excitation frequency

Conclusion and Discussion

This paper proposed a real-time monitoring method for the road-base quality (MRBQ), and its feasibility and accuracy has been identified. The soil dynamic model was extended with a piezoelectric equation to calculate the voltage in the road-base generated by a moving traffic load. The model test for the road-base under an excitation load was performed and a resonance column test (RCT) was conducted to measure the

road-base modulus. In the end, the road-base modulus back-calculated through the soil dynamic model was compared with measured road-base modulus by RCT, which verified the feasibility and accuracy of the proposed MRBQ. In the MRBQ, the sensitivity of the piezoelectric sensors can reach 2 V/MPa and the error between back-calculated and measured modulus is less than 20%. Additionally, the precision of the MRBQ can be enhanced as the traffic load amplitude and speed increases. Moreover, the effect of factors including excitation load amplitude, excitation frequency and road-base modulus on the electric response of piezoelectric sensors at various depth had been identified.

The proposed MRBQ shows good potential for application in the health monitoring of the transportation facilities under various circumstances due to its following advantages. First, the MRBQ can serve as an important component of road-base management system, which can realize the real-time monitoring of the road-base quality. Furthermore, the service life of the road-base can be predicted according to the attenuation curve of the road-base modulus. Second, to promote the construction of intelligent transportation system (ITS), the MRBQ can be used in combination with weight-in-motion (WIM) technology to grasp the traffic conditions on the road. Third, the modelling framework and the measurement methods of the MRBQ can supply guidelines for the real-time monitoring of other civil engineering structures.

This paper proposed a framework for the real-time monitoring method of the road-base, while there are also limitations: (1) Environmental factors have an important impact on real-time monitoring (Liu et al.,2019). The temperature and the road-base

water content can affect the results of the sensor (Yang et al.,2017), which needs to be further calibrated and insulation countermeasures. (2) The performance of MRBQ needs to be further verified in the real road-base and traffic environment.

Declaration of conflicting interests

The authors declared no potential conflicts of interest with respect to the research, authorship, and/or publication of this article.

Data Accessibility Statement

All data, models, and code generated or used during the study appear in the submitted article.

Funding

The authors wish to acknowledge the support of the National Natural Science Foundation of China (Grant Nos. 51778571, 51978611).

References

Auersch L (1996) Dynamic plate-soil interaction-finite and infinite, flexible and rigid plates on homogeneous, layered or Winkler soil. *Soil Dynamics and Earthquake Engineering* 15(1): 51-59.

Biot MA (1956) Theory of propagation of elastic waves in a fluid-saturated porous solid. II. Higher frequency range. *The Journal of the Acoustical Society of America* 28(2): 179-191.

Bo JIN (2004) Dynamic response of poroelastic half-space generated by high speed load (in Chinese). *Chinese Quarterly of Mechanics* 25(2): 168-174.

Cai Y, Cao Z, Sun H, et al. (2009) Dynamic response of pavements on poroelastic half-space soil medium to a moving traffic load. *Computers and Geotechnics* 36(1-2): 52-60.

Cai Y, Chen Y, Cao Z, et al. (2015) Dynamic responses of a saturated poroelastic half-space generated by a moving truck on the uneven pavement. *Soil Dynamics and Earthquake Engineering* 69: 172-181.

Cai Y, Sun H and Xu C (2007) Steady state responses of poroelastic half-space soil medium to a moving rectangular load. *International Journal of Solids and Structures* 44(22-23): 7183-7196.

Cao Z, Chen J, Cai Y, et al. (2018) Long-term behavior of clay-fouled unbound granular materials subjected to cyclic loadings with different frequencies. *Engineering Geology* 243: 118-127.

Danesh A, Palassi M and Mirghasemi AA (2018) Effect of sand and clay fouling on the shear strength of railway ballast for different ballast gradations. *Granular Matter* 20(3): 51.

Jia XM and Li B (2012) Study on application of Rayleigh wave in over coarse-grained subgrade detection (in Chinese). *Subgrade Engineering* 5:118-120.

Jin L, Zhang B, Zhang L, et al. (2019) Nanogenerator as new energy technology for self-powered intelligent transportation system. *Nano Energy* 66:104086.

Kafle B, Zhang L, Mendis P, et al. (2017) Monitoring the dynamic behavior of the Merlynston creek bridge using interferometric radar sensors and finite element modeling. *International Journal of Applied Mechanics* 9(1): 1750003.

Lin L, Hu Y, Xu C, et al. (2013) Transparent flexible nanogenerator as self-powered sensor for transportation monitoring. *Nano Energy* 2(1): 75-81.

Liu Z, Liu P, Zhou C, et al. (2019) Structural health monitoring of underground structures in reclamation area using fiber bragg grating sensors. *Sensors* 19(13):2849.

Lytton RL (1988) Backcalculation of pavement layer properties. In: *Nondestructive Testing of Pavements and Backcalculation of Moduli*. STP 1026, ASTM, Philadelphia, Pa., pp. 7-38.

Malla RB and Joshi S (2008) Subgrade resilient modulus prediction models for coarse and fine-grained soils based on long-term pavement performance data. *International Journal of Pavement Engineering* 9(6): 431-444.

Scrivner FH, Moore WM, Mcfarland WF, et al. (1968) *A systems approach to the flexible pavement design problem*. Report no. 32-11, Texas Transportation Institute, US, October.

Sun X, Han J, Crippen L, et al. (2016) Back-calculation of resilient modulus and prediction of permanent deformation for fine-grained subgrade under cyclic loading. *Journal of Materials in Civil Engineering* 29(5):04016284.

Ummin O, Qi YJ, Zhao JJ, et al. (2013) The application of the Rayleigh Wave in subgrade layer

detection. *Advanced Materials Research* 838-841: 1186-1190.

Wang J, Zhang H, Xie Y, et al. (2017) Smart network node based on hybrid nanogenerator for self-powered multifunctional sensing. *Nano Energy* 33: 418-426.

Wang S, Lin L and Wang ZL (2015) Triboelectric nanogenerators as self-powered active sensors. *Nano Energy* 11: 436-462.

Wang ZL (2013) Triboelectric nanogenerators as new energy technology for self-powered systems and as active mechanical and chemical sensors. *ACS Nano* 7(11): 9533-9557.

Xue W, Wang L, Wang D, et al. (2014) Pavement health monitoring system based on an embedded sensing network. *Journal of Materials in Civil Engineering* 26(10): 04014072.

Yang H, Guo M, Wang L, et al. (2017) Investigation on the factors influencing the performance of piezoelectric energy harvester. *Road materials and pavement design* 18(sup3):180-189.

Yu H, He X, Ding W, et al. (2017) A self-powered dynamic displacement monitoring system based on triboelectric accelerometer. *Advanced Energy Materials* 7(19): 1700565.

Zhang Z, Xiang H and Shi Z (2015) Modeling on piezoelectric energy harvesting from pavements under traffic loads. *Journal of intelligent material systems and structures* 27(4): 567-578.

Zhao X, Wei G, Li X, et al. (2017) Self-powered triboelectric Nano vibration accelerometer based wireless sensor system for railway state health monitoring. *Nano Energy* 34: 549-555.